Available online at www.sciencedirect.com
SCIENCE DIRECT®
Scripta Materialia 52 (2005) 911–915
Scripta MATERIALIA
www.actamat-journals.com

Characterization and modeling of localized compaction in aluminum foam

K.A. Issen *, T.P. Casey, D.M. Dixon, M.C. Richards, J.P. Ingraham

Department of Mechanical and Aeronautical Engineering, Clarkson University, Potsdam, NY 13699-5725, USA

Received 24 August 2004; received in revised form 13 December 2004; accepted 28 December 2004
Available online 26 January 2005

Abstract

Uniaxial compression tests on aluminum foam reveal formation of bands of localized compaction, initiating near peak stress, and becoming clearly defined during the subsequent stress drop. Band formation is modeled as a bifurcation from uniform deformation due to a constitutive instability. Theoretical predictions and experimental observations are in reasonable agreement.

Keywords: Compression test; Aluminum; Foams; Yield phenomena; Analytical methods

1. Introduction

Porous solids are becoming an increasingly important class of materials. Closed cell aluminum foams, for example, are lightweight, buoyant, recyclable, non-toxic, non-flammable and have good mechanical damping characteristics and sound absorbing capacities [1]. However, before potential applications can be realized, a thorough understanding of the mechanical behavior of these materials is required. The typical uniaxial compressive stress–strain response of porous cellular materials consists of near-linear loading that leads to a stress peak, followed by a stress drop, and then a long stress plateau region where much of the porosity is crushed out, after which, the stress increases with increasing strain [2]. This characteristic behavior is useful in energy absorbing applications, but could be catastophic in structural applications. Zones of localized compaction, "compaction bands", have been observed in aluminum foams [3–6] and steel foams [7]. These bands typically form approximately perpendicular to the axial compression direction and consist of predominantly axial strain, resulting from cell collapse. Bands of compaction, oriented perpendicular to uniaxial loading, also occur in polycarbonate and aluminum honeycombs [8,9]. A similar deformation mode, also referred to as a compaction band, occurs in high porosity sandstone under axisymmetric compression [10,11]; however, the porosity reduction mechanism is grain crushing and pore collapse. In this work, surface strain mapping is employed to examine the onset of localized compaction, and experimental observations are compared with theoretical predictions for band formation, developed using bifurcation theory.

2. Experimental procedure

Specimens were cut from Cymat structural grade aluminum foam to dimensions 27 mm × 27 mm × 54 mm, using wire electro-discharge machining per ASTM standards [12]. These specimens had an average relative density of 0.17 and typical cell sizes ranging from 2 to 6 mm in diameter. However, significant variation in local density as well as cell size and shape are clearly observable

* Corresponding author. Tel.: +1 315 268 3880; fax: +1 315 268 6695.
E-mail address: issenka@clarkson.edu (K.A. Issen).

1359-6462/$ - see front matter
doi:10.1016/j.scriptamat.2004.12.031

on cut faces. One face of each specimen was painted with black and white speckles and illuminated with a fiber optic white light source, to facilitate digital image correlation. Ends were lubricated to reduce friction and specimens were subjected to quasistatic (2.7×10^{-6} m/s) uniaxial compression using displacement control. A Kodak ES 1.0 camera with a 1008×1012 pixel CCD sensor acquired one image per second, while load cell and cross head displacement data were recorded. Several unloading loops were performed before peak stress, to determine the elastic Young's modulus and Poisson's ratio prior to compaction band formation. Full field surface strain contour plots of axial, lateral and shear strain were created at regular displacement intervals, using VIC-2D digital image correlation software [13]. Specimens were loaded past the stress peak and stress drop, well into the plateau region, until the compaction band was clearly visible on the specimen face. This process enabled visual confirmation of the compaction band location shown in the axial surface strain contour plots. Due to difficulties in attaching physical strain measurement devices to the specimen, the virtual extensometer feature of VIC-2D was used to determine average axial and lateral strains for the bulk specimen response.

3. Experimental results

Results from a representative specimen (C5a18) are shown in Fig. 1. The stress–strain plot shows nominal stress (force divided by original cross sectional area) vs. nominal strain (cross head displacement divided by original length), both positive in compression. The three axial surface strain contour plots relate to the three loading stages, *A* (pre-peak), *B* (peak), and *C* (post-peak), labeled on the stress–strain plot. Because the current work focuses on compaction band initiation, the stress–strain curve is shown only through the stress drop, although all specimens were loaded to approxi-

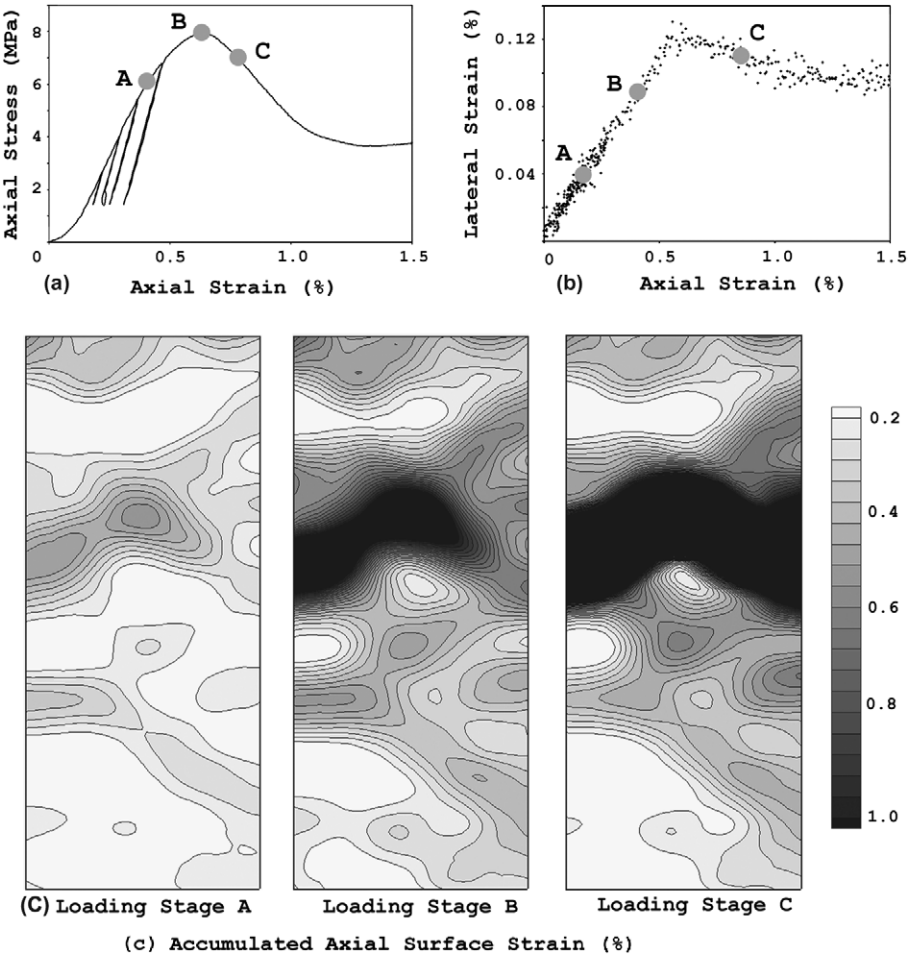

Fig. 1. (a) Nominal stress–nominal strain curve (positive in compression) for specimen C5a18; (b) lateral strain vs. axial strain (slope, $v_t \approx 0$, just after peak stress); (c) axial surface strain maps corresponding to loading stages A, B, and C shown in (a). (A): Prior to peak stress, deformation consists of isolated zones of compaction. (B) Peak stress, strain is localizing in the compaction band zone. (C) Post-peak, compaction band is clearly defined.

mately 5% axial strain. The complete stress–strain plots, characterized by a large stress drop and jagged sloping plateau, are similar to those reported by other authors for brittle foams [3,14,15]. From the four unloading loops, note that the material unloads and reloads on a stiffer curve than the initial loading curve, implying that inelastic deformation occurs early in the loading program. Similar findings by others suggest that the near-linear portion of loading curve is not elastic [3,6,14,16,17]. Using the nominal stress and virtual extensometer strain data for the unloading loops, the elastic Young's modulus and Poisson's ratio for the specimens were found to be 3.6–4.9 GPa and 0.11–0.26, respectively.

The gray-scale contour plots (Fig. 1) show accumulated surface axial strain, with progressively darker shades representing increasingly compressive strain. At loading stage *A*, prior to peak stress, deformation consists of multiple isolated zones of localized compaction, distributed across the specimen face. At peak stress, *B*, strain begins to localize into a single zone of localized axial compaction. During the stress drop, *C*, a large portion of the specimen shortening goes into the compaction band, which is now well defined. Comparing strain maps for *B* and *C* reveal several zones of local unloading (e.g., left side above band) that occur during the stress drop, as the specimen continues to shorten. Fig. 1 also shows evolution of the "total" Poisson's ratio, v_t (the negative of the ratio of the lateral and axial strain increments, including elastic and inelastic portions), which will be utilized in the theoretical predictions. Through peak stress, v_t is relatively constant, and then decreases rapidly such that $v_t \approx 0$ shortly after peak stress.

Although the compaction band in Fig. 1 appears to be roughly perpendicular to the axial direction (band angle of ≈0°, where the band angle is defined as the angle between the band normal and the axial direction), determination of the observed band angle also requires examination of the non-photographed faces. For each specimen, the observed band angle was estimated by fitting a plane through the four points where the band intersected the corners of the specimen. Clearly this method is an approximation, however, since the exact location of the band inside the specimen is also unknown, this method was deemed adequate to provide an initial estimate of the band angle. In future work, X-ray computed tomography could facilitate more accurate determination of band angle. The estimated observed band angles (see Table 1) range from 8° to 16°.

Table 1
Observed and predicted band angles

Sample	Band angles	
	Observed (deg)	Predicted (deg)
C5a4	16	19
C5a5	9	17
C5a7	14	8
C5a9	16	20
C5a11	9	14
C5a15	11	19
C5a17	13	14
C5a18	8	17

Data for specimen C5a18 is shown in Fig. 1.

4. Localization theory

Bands of localized compaction have also been observed in field and laboratory specimens of high porosity sandstone subject to axisymmetric compression [10,11,18]. The undeformed porosities of these sandstones range from 13% to 28%. Similar to the compaction bands observed here, those in sandstone form perpendicular to the direction of maximum compression, but are composed of crushed grains and collapsed pores, resulting in reduced porosity and reduced permeability [19]. Olsson [10] suggested that compaction band formation in sandstone could be predicted using the localization theory of Rudnicki and Rice [20], originally developed for shear localization in low porosity rock. Rudnicki and Rice suggested that the inception of a planar band of localized deformation could be viewed as a bifurcation from continued homogenous deformation, due to a constitutive instability. The localization condition is given by $\det|n_i\, L_{ijkl}\, n_l| = 0$, where n_i are the components of the band normal and L_{ijkl} is the modulus tensor in the incrementally linear stress–strain relationship, $d\sigma_{ij} = L_{ijkl} d\varepsilon_{kl}$ (elastic and inelastic strains are included in $d\varepsilon_{kl}$).

Clearly the localization conditions are influenced by the choice of constitutive relation. For porous rock, Issen and Rudnicki [21] assume a yield function, $F(\tau, \sigma, \alpha_\kappa) = 0$, which depends on the first invariant of stress through $\sigma = -\sigma_{kk}/3$ and the second invariant of deviatoric stress through $\tau = (s_{ij}s_{ij}/2)^{1/2}$, where the deviatoric stress is $s_{ij} = \sigma_{ij} - \sigma_{kk}\delta_{ij}/3$, and the α_κ are a set of variables used to track inelastic deformation. If non-associated flow is applicable, a plastic potential, normal to the inelastic strain increments, is also required. The constitutive relations of Rudnicki and Rice can be derived using this formulation [22,23]. Although developed for dilatant materials, a more general form of the pressure sensitive Rudnicki and Rice constitutive framework is obtained by allowing μ and β (the slopes of the yield surface and plastic potential, respectively, in σ–τ stress space) to be positive (dilatant) or negative (compactant). Such a negatively sloping yield surface was proposed for metal foams by Deshpande and Fleck [24], who employed a plasticity approach with associated flow to develop constitutive relations for metal foams. Their yield

function is represented by a quarter ellipse in $\sigma_m - \sigma_e$ stress space ($\sigma_m = \sigma_{kk}/3$, and $\sigma_e = (3s_{ij}s_{ij}/2)^{1/2}$).

Issen and Rudnicki [25] examined the conditions for formation of a planar band of localized deformation in compactant materials, using the Rudnicki and Rice constitutive relations. For the axisymmetric compression stress state (principal stresses: $0 \geqslant \sigma_I = \sigma_{II} \geqslant \sigma_{III}$), compaction bands with a band angle of 0° are predicted when $\beta + \mu \leqslant -\sqrt{3}$ (for associated flow, the condition becomes $\beta = \mu \leqslant -\sqrt{3}/2$). When this condition is violated, the predicted band angle is: $\theta = \pi/4 + (1/2)\arcsin\{[2\sqrt{3}(1+\nu)(\beta+\mu) - (1-2\nu)]/9\}$ ([26], specialized for axisymmetric compression). Using a similar bifurcation approach, Rudnicki [27] determined conditions for compaction band formation in transversely isotropic materials under axisymmetric compression. Rudnicki found that compaction band formation is predicted when $E_t + 9Kr\nu_t/2 = 0$, where E_t is the tangent modulus of the axial stress–axial strain curve, ν_t is the total Poisson's ratio, r is the ratio of axial stress increment to lateral stress increment for zero axial strain increment, and $9K$ relates increments of lateral strain to increments of lateral stress for zero axial strain. If a compaction band forms at approximately peak stress, then $E_t \approx 0$ and theory predicts that at least one of ν_t, r, or K must also be zero.

5. Discussion

The slope of the plastic potential for axisymmetric (or uniaxial) compression is given by $\beta = -\sqrt{3}b/(3-b)$, where b is the ratio of the inelastic volume strain, $d\varepsilon_v^p$, to inelastic axial strain $d\varepsilon_a^p$ (both positive in compression), $b = d\varepsilon_v^p/d\varepsilon_a^p$ [28]. Using these values of β, and assuming associated flow [24], $\mu = \beta$, the predicted band angle, θ, was calculated from the equation given above. Since surface strain maps suggest that the band forms near peak stress, the predicted band angles at peak stress were calculated and are found to range from 8° to 20°, while estimated observed band angles are 8–16° (see Table 1). This reasonably favorable agreement is noteworthy, considering the difficulties and assumptions (discussed next) involved in determining predicted and observed band angles. Additionally, at peak stress, E_t is zero, and from Fig. 1, notice that ν_t, the slope of the lateral vs. axial stress curve, goes to zero slightly past the stress peak. These observations compare favorably with Rudnicki's predictions of compaction band formation in transversely isotropic materials at peak stress ($E_t = 0$), if $\nu_t = 0$ [27].

Since only uniaxial tests were conducted, the yield surface slope, μ, cannot be determined, so associated flow, $\mu = \beta$, was assumed. However, band angle predictions would change if $\mu \neq \beta$. Additionally, the theoretical continuum approach used here assumes that the specimen size to cell size ratio is large. While the specimens studied here satisfy the suggested conditions for bulk material behavior (i.e., a minimum specimen dimension is six to 10 cells [29]), significant variation exists between specimens, and the observed bands were not strictly planar, as predicted by localization theory. (This also complicates estimation of observed band angles.) The specimen size to cell size ratio used here is roughly 7:1. However, in sandstone specimens, where the specimen width to grain diameter ratio is 250, clearly planar bands are observed [10]. Therefore, larger metal foam specimens may be required to observe true continuum behavior. Additionally, a more sophisticated method, such as X-ray computed tomography, could be used to more accurately determine actual band angles.

The Cymat manufacturing process results in denser material at the foam panel faces (corresponding to the specimen ends), such that compaction localization typically occurs in the less dense middle section of the specimen. Certainly this density gradient, as well as the inhomogeneous cell microstructure (in particular, certain cell geometries that are prone to collapse, see Refs. [3,5,6,14,30–34]), result in conditions that favor compaction localization. While inhomogeneities are often identified as the cause of compaction localization, we present an alternate perspective: compaction localization can be viewed as a constitutive instability for compacting porous materials (a bifurcation from homogenous deformation), which is possible even for materials with "perfect" microstructure and uniform density. Therefore, while the material studied here exhibits significant inhomogeneities that clearly promote compaction band formation, we suggest that the underlying constitutive instability enables the alternate deformation mode (compaction localization), and that ever-present material defects (including density variations) cause this mode to be favored over homogenous deformation. Thus, compaction band formation may be a common, or perhaps inevitable, deformation mode in porous materials. Since the continuum approach employed in this work is independent of microstructure, it could be applied toward predicting compaction localization in various porous materials with differing microstructures.

6. Conclusions

Uniaxial compression tests on aluminum foam reveal the formation of bands of intense localized compaction, "compaction bands", oriented approximately perpendicular to the loading direction. Digital image correlation was used to produce maps of surface axial strain, which show that near peak stress the deformation mode transitions from multiple zones of isolated compaction, to a single compaction band. The stress peak is followed by a large stress drop, during which a significant amount

of the specimen shortening is absorbed by a band, which becomes clearly defined. Some unloading is observed in material outside the band. The theoretical framework developed by Rudnicki and Rice [20] for strain localization in low porosity rock, which has been used to predict compaction band formation in high porosity sandstone [10,21,23,25,27], was applied to predict compaction localization in the aluminum foam studied here. Using this approach, band formation is modeled as a bifurcation from uniform deformation, due to a constitutive instability. Theoretical predictions and experimental observations regarding band formation and orientation were found to be in reasonable agreement. Predicted band angles ranged from 8° to 20°, while estimated observed band angles were 8 to 16°. These findings suggest that bifurcation theory is a promising approach for modeling the inception of compaction bands, which could be a common deformation mode for high porosity materials.

Acknowledgments

The authors would like to thank Jeffrey A. Taylor and David J. Morrison of Clarkson University, Huber Schreier of Correlated Solutions, Inc. and William A. Olsson of Sandia National Laboratories for helpful discussions regarding digital image correlation and compression testing. We also acknowledge financial support from the National Science Foundation, Directorate of Engineering, Division of Civil and Mechanical Systems, Mechanics and Structures of Materials Program, award CMS-0422045 to Clarkson University.

References

[1] Ashby MF, Evans A, Fleck NA, Gibson LJ, Hutchinson JW, Wadley HNG. Metal foams: A design guide. Oxford: Butterworth–Heinemann; 2000.
[2] Gibson JL, Ashby MF. Cellular solids structure and properties. New York: Cambridge University Press; 1997.
[3] Andrews E, Sanders W, Gibson LJ. Mater Sci Eng A 1999;270:113–24.
[4] Gradinger R, Rammerstofer FG. Acta Mater 1999;47(1):143–8.
[5] Bart-Smith H, Bastawros A-F, Mumm DR, Evans AG, Sypeck DJ, Wadley HNG. Acta Mater 2000;46(10):3583–92.
[6] Bastawros A-F, Bart-Smith A, Evans AG. J Mech Phys Solids 2000;28:301–22.
[7] Park C, Nutt SR. Mater Sci Eng A 2001;299:68–74.
[8] Papka SD, Kyriakides S. Int J Solids Struct 1998;35(3-4):239–67.
[9] Papka SD, Kyriakides S. Acta Mater 1998;46:2765–76.
[10] Olsson WA. J Geophys Res 1999;104:7219–28.
[11] Wong T-f, Baud P, Klein E. Geophys Res Lett 2001;28(13):2521–4.
[12] ASTM E9-89a, Standard Test Methods of Compression Testing of Metallic Materials at Room Temperature.
[13] VIC2D digital image correlation software, Correlated Solutions, Inc., West Columbia, SC.
[14] Sugimura Y, Meyer J, He MY, Bart-Smith H, Grenstedt J, Evans AG. Acta Mater 1997;45(12):5245–59.
[15] Markaki AE, Clyne TW. Acta Mater 2001;49:1677–86.
[16] McCullough KYG, Fleck NA, Ashby MF. Acta Mater 1999;47(8):2323–30.
[17] Gioux G, McCormack TM, Gibson JL. Int J Mech Sci 2000;42:1097–117.
[18] Mollema PN, Antonellini MA. Tectonophysics 1996;267:209–28.
[19] Holcomb DJ, Olsson WA. J Geophys Res 2001;108(B6):2290.
[20] Rudnicki JW, Rice JR. J Mech Phys Solids 1975;23:371–94.
[21] Issen KA, Rudnicki JW. Phys Chem Earth (A) 2001;26(1–2):95–100.
[22] Holcomb DJ, Rudnicki JW. Int J Numer Anal Methods Geomech 2001;25:109–29.
[23] Issen KA. Eng Fract Mech 2002;69:1891–906.
[24] Deshpande VS, Fleck NA. J Mech Phys Solids 2000;48:1253–83.
[25] Issen KA, Rudnicki JW. J Geophys Res 2000;105:21529–36.
[26] Rudnicki JW, Olsson WA. Int J Rock Mech Min Sci 1998;35:4–5.
[27] Rudnicki JW. Int J Solids Struct 2002;39(13–14):3741–56.
[28] Wong T-f, David C, Zhu W. J Geophys Res 1997;102:3009–25.
[29] Andrews EW, Gioux G, Onck P, Gibson LJ. Int J Mech Sci 2001;43:701–13.
[30] Simone AE, Gibson LJ. Acta Mater 1998;46(9):3109–23.
[31] Simone AE, Gibson LJ. Acta Mater 1998;46(11):3929–35.
[32] Grenestedt JL. J Mech Phys Solids 1998;46(1):29–50.
[33] Grenestedt JL, Bassinet F. Int J Mech Sci 2000;42:1327–38.
[34] Olurin OB, Fleck NA, Ashby MF. Mater Sci Eng A 2000;291:136–46.